10022 *Inorg. Chem.* **2010**, *49*, 10022–10031
DOI: 10.1021/ic101304v

Inorganic Chemistry
Article

Spin-Crossover and Liquid Crystal Properties in 2D Cyanide-Bridged $Fe^{II}-M^{I/II}$ Metalorganic Frameworks[▽]

M. Seredyuk,[†,⊥] A. B. Gaspar,*[,‡] V. Ksenofontov,[†] Y. Galyametdinov,[§] M. Verdaguer,[∥] F. Villain,[∥] and P. Gütlich*[,†]

[†]*Institut für Anorganische und Analytische Chemie, Johannes-Gutenberg-Universität, Staudinger-Weg 9, D-55099 Mainz, Germany,* [‡]*Institut de Ciència Molecular (ICMOL)/Departament de Química Inorgànica, Universitat de València, Edifici de Instituts de Paterna, Apartat de Correus 22085, 46071 València, Spain,* [§]*Kazan Physical Technical Institute, Russian Academy of Science, Sibirsky Tract 10/7, 420029, Kazan, Russia, and* [∥]*Institut Parisien de Chimie Moléculaire, UMR CNRS 7201, FR-CNRS 2769, Université Pierre et Marie Curie, 4 place Jussieu, case courrier 42, 75252 Paris Cedex 05, France.* [⊥]*On leave from Kiev National University*

Received June 29, 2010

Novel two-dimensional heterometallic Fe(II)−M(Ni^{II}, Pd^{II}, Pt^{II}, Ag^{I}, and Au^{I}) cyanide-bridged metalorganic frameworks exhibiting spin-crossover and liquid crystal properties, formulated as $\{FeL_2[M^{I/II}(CN)_x]_y\}\cdot sH_2O$, where L are the ligands 4-(4-alkoxyphenyl)pyridine, 4-(3,4-dialkoxyphenyl)pyridine, and 4-(3,4,5-trisalkoxyphenyl)pyridine, have been synthesized and characterized. The physical characterization has been carried out by means of EXAFS, X-ray powder diffraction, magnetic susceptibility, differential scanning measurements, and Mössbauer spectroscopy. The 2D Fe(II) metallomesogens undergo incomplete and continuous thermally induced spin transition at $T_{1/2} \approx 170$ K and crystal-to-smectic transition above 370 K.

Introduction

Spin-crossover (SCO) compounds represent a type of functional molecular material with labile electronic configurations switchable between the high-spin (HS) and low-spin (LS) states in response to external stimuli (temperature,[1] pressure,[2] light,[3] magnetic field,[1a,e] or guest absorption/desorption[4]). In the HS and LS states, SCO compounds manifest differences in magnetism, optical properties, dielectric constant, color, and structure. These characteristics have made the SCO phenomenon one of the most interesting application-oriented examples of bistability in molecular materials.[2b−d,4c,e,f,5]

The SCO phenomenon has recently been investigated in the framework of other materials of technological interest such as liquid crystals.[5] Materials combining spin-crossover and liquid crystalline behavior may lead to a number of advantages in practical applications, for example, processing spin-crossover materials in the form of thin films, enhancement of spin transition signals, switching and sensing in different temperature regimes, or the achievement of photo- and thermochromism in Fe(II)-containing liquid crystals. The change of color is certainly a phenomenon which is of interest in the field of liquid crystals. The interest lies in the necessity of color change in a number of applications in liquid crystals such as passive blocking filters, laser addressed devices, polarizers based on dichroic effects, or the utility of thermochromism.[6]

[▽] Dedicated to Professor Wolfgang Kaim on the occasion of his 60th birthday.

*To whom correspondence should be addressed. E-mail: ana.b.gaspar@uv.es (A.B.G.).

(1) (a) Gütlich, P.; Goodwin, G. *Top. Curr. Chem.* **2004**, *233*; *234*; *235*. (b) Gaspar, A. B.; Ksenofontov, V.; Seredyuk, M.; Gütlich, P. *Coord. Chem. Rev.* **2005**, *249*, 2661. (c) Real, J. A.; Gaspar, A. B.; Muñoz, M. C. *Dalton Trans.* **2005**, 2062. (d) Real, J. A.; Gaspar, A. B.; Niel, V.; Muñoz, M. C. *Coord. Chem. Rev.* **2003**, *236*, 121. (e) Gütlich, P.; Hauser, A.; Spiering, H. *Angew. Chem., Int. Ed.* **1994**, *33*, 2024.

(2) (a) Gütlich, P.; Ksenofontov, V.; Gaspar, A. B. *Coord. Chem. Rev.* **2005**, *249*, 1811. (b) Galet, A.; Gaspar, A. B.; Muñoz, M. C.; Bukin, G. V.; Levchenko, G.; Real, J. A. *Adv. Mater.* **2005**, *17*, 2949. (c) Kahn, O.; Martinez, J. *Science* **1998**, *279*, 44. (d) Kahn, O.; Kröber, C.; Jay, C. *Adv. Mater.* **1992**, *4*, 718.

(3) (a) Decurtins, S.; Gütlich, P.; Köhler, C. P.; Spiering, H.; Hauser, A. *Chem. Phys. Lett.* **1984**, *105*, 1. (b) Trzop, E.; Cointe, M. B. L.; Cailleau, H.; Toupet, L.; Molnar, G.; Bousseksou, A.; Gaspar, A. B.; Real, J. A.; Collet, E. *J. Appl. Crystallogr.* **2007**, *40*, 158. (c) Létard, J. F. *J. Mater. Chem.* **2006**, *16*, 2550. (d) Bonhommeau, S.; Molnar, G.; Galet, A.; Zwick, A.; Real, J. A.; McGarvey, J. J.; Bousseksou, A. *Angew. Chem., Int. Ed.* **2005**, *44*, 4069.

(4) (a) Real, J. A.; Andres, E.; Muñoz, M. C.; Julve, M.; Granier, T.; Bousseksou, A.; Varret, F. *Science* **1995**, *268*, 265. (b) Neville, S. M.; Halder, G. J.; Chapman, K. W.; Duriska, M. B.; Southon, P. D.; Cashion, J. D.; Letard, J. F.; Moubaraki, B.; Murray, K. S.; Kepert, C. J. *J. Am. Chem. Soc.* **2008**, *130*, 2869. (c) Agustí, G.; Ohtani, R.; Yoneda, K.; Gaspar, A. B.; Ohba, M.; Muñoz, M. C.; Kitagawa, S.; Real, J. A. *Angew. Chem., Int. Ed.* **2009**, *48*, 8944. (d) Neville, S. M.; Halder, G. J.; Chapman, K. W.; Duriska, M. B.; Moubaraki, B.; Murray, K. S.; Kepert, C. J. *J. Am. Chem. Soc.* **2009**, *131*, 12106. (e) Ohba, M.; Yoneda, K.; Agusí, G.; Munoz, M. C.; Gaspar, A. B.; Real, J. A.; Yamasaki, M.; Ando, H.; Nakao, Y.; Sakaki, S.; Kitagawa, S. *Angew. Chem., Int. Ed.* **2009**, *48*, 4767. (f) Southon, P. D.; Liu, L.; Fellows, E. A.; Price, D. J.; Halder, G. J.; Chapman, K. W.; Moubaraki, B.; Murray, K. S.; Letard, J.-F.; Kepert, C. J. *J. Am. Chem. Soc.* **2009**, *130*, 10998.

(5) Gaspar, A. B.; Seredyuk, M.; Gütlich, P. *Coord. Chem. Rev.* **2009**, *253*, 2399.

(6) (a) Hudson, S. A.; Maitlis, P. M. *Chem. Rev.* **1993**, *93*, 861. (b) Serrano, J. L. *Metallomesogens*; VCH: Weinheim, Germany, 1996. (c) Donnio, B.; Bruce, D. W. *Struct. Bonding* (*Berlin*) **1999**, *95*, 193. (d) Bruce, D. W. *Acc. Chem. Res.* **2000**, *33*, 831. (e) Lemieux, R. P. *Acc. Chem. Res.* **2001**, *34*, 845. (f) Donnio, B. *Curr. Opin. Colloid, Interface Sci. State Mater. Sci.* **2002**, *7*, 371. (g) Gimenez, R.; Lydon, D. R.; Serrano, J. L. *Curr. Opin. Solid State Mater. Sci.* **2002**, *6*, 527. (h) Serrano, J. L.; Sierra, T. *Coord. Chem. Rev.* **2003**, *242*, 73. (i) Piguet, C.; Bunzli, J. C. G.; Donnio, B.; Guillon, D. *Chem. Commun.* **2006**, 3755.

 Published on Web 09/30/2010

Scheme 1. Structure of Fe(II) Metallomesogens under Study and Their Codes[a]

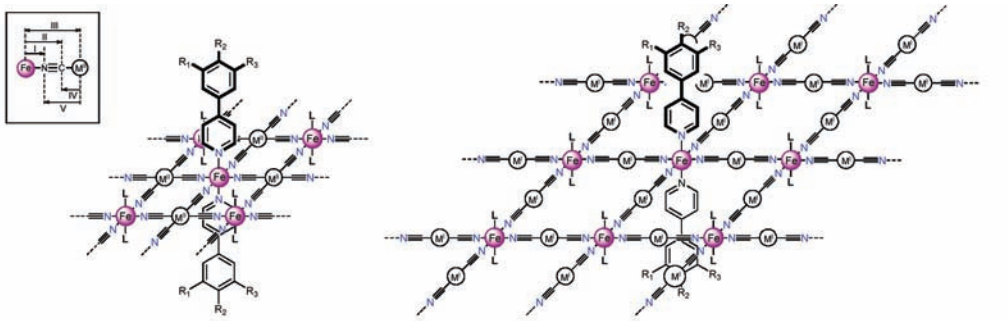

	Substituents	Ligand	Metal $M^{I/II}$				
			Ni^{II}	Pd^{II}	Pt^{II}	Ag^{I}	Au^{I}
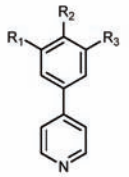	$R_1 = R_3 = H$, $R_2 = -OC_nH_{2n+1}$	4-C6	**1** (1)[b]				**18** (1)
		4-C18	**2** (1)	**6** (1)	**10** (1)	**14** (0.5)	**19** (0.5)
		4-C12	**3** (0.5)	**7** (1)	**11** (1)	**15** (0.5)	**20** (0)
	$R_1 = R_2 = -OC_nH_{2n+1}$, $R_3 = H$	34-C12	**4** (2)	**8** (0.5)	**12** (1)	**16** (1)	**21** (2)
	$R_1 = R_2 = R_3 = -OC_nH_{2n+1}$	345-C12	**5** (2)	**9** (3)	**13** (2)	**17** (2)	**22** (0.5)

[a] The roman numerals above the arrows indicate the scattering pathways at the iron *K* edge (I, II, III) and nickel *K* edge (IV, V, III) observable in the EXAFS Fourier transforms. [b] In parentheses are given the numbers of the crystal water molecules deduced from TGA.

Recently, we have illustrated the strategies developed in order to achieve interplay/synergy between spin transition and liquid crystal transition.[5,7] The synthesized Fe(II) metallomesogens exhibit different types of interplay between both phase transitions. A classification according to the analysis of the magnetic and structural data has led to the distinction of three types of interplay, namely, type i, systems with coupling between the electronic structure of the iron(II) ions and the mesomorphic behavior of the substance; type ii, systems where both transitions coexist in the same temperature region but are not coupled due to competition with the dehydration (release of crystal water on heating); type iii, systems where both transitions occur in different temperature regions and therefore are uncoupled.

So far, these investigations have been centered in mononuclear[7b,c] and one-dimensional Fe(II) metallomesogens.[7a,8] In this regard, we aimed to explore the possibility to achieve similar physical properties by modifying chemically the two-dimensional cyanide-bridged Hoffman-like Fe(II) SCO polymers $\{Fe(4\text{-Phpy})_2[M^{II/I}(CN)_x]_y\}\cdot sH_2O$ (4PhyPy = 4-phenylpyridine; M^{II} = Ni, Pd, Pt; M^{I} = Ag, Au).[9] These complexes were synthesized and studied because they might be well suited for grafting the liquid crystal chemical functionality without substantial perturbation of the polymeric arrays. Here, we report the chemical modification of these Fe(II) coordination polymers that lead to the isolation of the corresponding Fe(II) metallomesogens formulated as $\{FeL_2[M^{II/I}(CN)_x]_y\}$, where L are the ligands 4-(4-alkoxyphenyl)pyridine, 4-(3,4-dialkoxyphenyl)-pyridine, and 4-(3,4,5-trisalkoxyphenyl)pyridine. We shall present and discuss the characterization of their spin-crossover and liquid crystal properties. Scheme 1 shows the structure of Fe(II) metallomesogens under study and their codes.

Experimental Section

Synthesis of Compounds. Starting reagents and solvents were obtained commercially from Aldrich or Across and used as received. The synthesis of $[N(t\text{-Bu})_4]_2[M^{II}(CN)_4]$ (M^{II} = Ni, Pd, Pt) and $[N(t\text{-Bu})_4][M^{I}(CN)_2]$ (M^{I} = Ag, Au) is described by Seredyuk et al.[9] The synthesis of ligands is summarized in Scheme 2.

Compounds 4-(4-methoxyphenyl)pyridine (**4A**), 4-(3,4-dimethoxyphenyl)pyridine (**34A**), and 4-(3,4,5-trismethoxyphenyl)pyridine (**345A**) were prepared using Suzuki-coupling according to the synthetic procedure described by Manley et al.[10]

Compound **4A**. Yield 74%. Found: C, 77.83; H, 6.04; N, 7.37. $C_{12}H_{11}NO$ requires: C, 77.81; H, 5.99; N, 7.56. *m*/*z* (EI): 185.1 $[M]^+$ (100%), 170.0 $(M-CH_3)^+$ (35%). ^{1}H NMR δ_H (400 MHz, $CDCl_3$): 8.56 (2H, dd, J = 2.0, 5.8 Hz, $PyH^{2,6}$), 7.56 (2H, dd, J = 1.2, 8.6 Hz, $PhH^{2,6}$), 7.43 (2H, dd, J = 2.0, 5.8 Hz, $PyH^{3,5}$), 6.98 (2H, dd, J = 1.2, 8.6 Hz, $PhH^{3,5}$), 3.83 (3H, s, OCH_3). ^{13}C NMR δ_C (100 MHz, $CDCl_3$): 158.4, 150.1, 146.7, 127.5, 125.9, 125.9, 115.8, 55.9.

Compound **34A**. Yield 61%. Found: C, 72.53; H, 6.03; N, 6.50. $C_{13}H_{13}NO_2$ requires: C, 72.54; H, 6.09; N, 6.51. *m*/*z* (EI): 215.2 $[M]^+$ (100%). ^{1}H NMR δ_H (400 MHz, $CDCl_3$): 8.58 (2H, dd, J = 1.2, 4.6 Hz, $PyH^{2,6}$), 7.43 (2H, dd, J = 1.2, 4.6 Hz, $PyH^{3,5}$), 7.19 (1H, dd, J = 0.2, 8.4 Hz, PhH^{6}), 7.10 (1H, J = 0.2 Hz, PhH^{2}), 6.93 (1H, J = 8.4 Hz, PhH^{5}), 3.92 (3H, s, OCH_3), 3.90 (3H, s, OCH_3). ^{13}C NMR δ_C (100 MHz, $CDCl_3$): 149.9, 149.8, 149.3, 147.9, 130.6, 121.0, 119.4, 111.4, 109.7, 55.8.

(7) (a) Seredyuk, M.; Gaspar, A. B.; Ksenofontov, V.; Reiman, S.; Galyametdinov, Y.; Haase, W.; Rentschler, E.; Gütlich, P. *Chem. Mater.* **2006**, *18*, 2513. (b) Seredyuk, M.; Gaspar, A. B.; Ksenofontov, V.; Galyametdinov, Y.; Kusz, J.; Gütlich, P. *J. Am. Chem. Soc.* **2008**, *130*, 1431. (c) Seredyuk, M.; Gaspar, A. B.; Ksenofontov, V.; Galyametdinov, Y.; Kusz, J.; Gütlich, P. *Adv. Funct. Mater.* **2008**, *18*, 2089.

(8) Seredyuk, M.; Gaspar, A. B.; Ksenofontov, V.; Galyametdinov, Y.; Verdaguer, M.; Villain, F.; Gütlich, P. *Inorg. Chem.* **2008**, *47*, 10232.

(9) Seredyuk, M.; Gaspar, A. B.; Ksenofontov, V.; Verdaguer, M.; Villain, F.; Gütlich, P. *Inorg. Chem.* **2009**, *48*, 6130.

(10) Manley, P. W.; Acemoglu, M.; Marterer, W.; Pachinger, W. *Org. Process Res. Dev.* **2003**, *7*, 436.

Scheme 2. Synthesis of the Ligands 4-Cn, 34-C12, 345-C12[a]

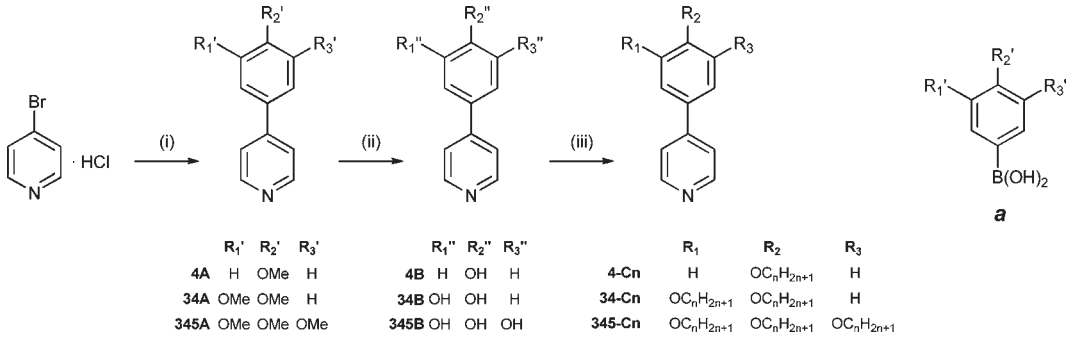

[a] Reagents and conditions: (i) **a**, K_2CO_3, $Pd(ac)_2$, (*o*-tol)$_3$P, $(CH_3OCH_2)_2$, 80 °C, 14 h; (ii) $HBr_{48\%}/CH_3COOH$ (1:1), reflux, 2 h; (iii) $C_nH_{2n+1}Br$, K_2CO_3, DMF, 100 °C, 8 h.

Compound **345A**. Yield 54%. Found: C, 68.57; H, 6.22; N, 5.69. $C_{14}H_{15}NO_3$ requires: C, 68.56; H, 6.16; N, 5.71. *m*/*z* (EI): 245.1 $[M]^+$ (100%). ^{1}H NMR δ_H (400 MHz, $CDCl_3$): 8.65 (2H, dd, J = 0.8, 7.0 Hz, PyH^{2,6}), 7.47 (2H, dd, J = 0.8, 7.0 Hz, PyH^{3,5}), 6.83 (2H, s, ArH), 3.94 (6H, s, OCH_3), 3.91 (3H, s, OCH_3). ^{13}C NMR δ_C (100 MHz, $CDCl_3$): 153.6, 149.9, 148.2, 138.8, 133.7, 121.4, 104.1, 60.8, 56.1.

Compounds 4-(4-hydroxyphenyl)pyridine (**4B**), 4-(3,4-dihydroxyphenyl)pyridine hydrobromide dihydride (**34B**), and 4-(3,4,5-trishydroxyphenyl)pyridine hydrobromide semihydride (**345B**) were prepared from compounds **4A**, **34A**, and **345A**, respectively, by ether cleavage according to the procedure described by Gessner et al.[11]

Compund **4B**. Yield 95%. Found: C, 77.19; H, 5.30; N, 8.30. $C_{11}H_9NO$ requires: C, 77.17; H, 5.30; N, 8.18. *m*/*z* (EI): 171.0 $[M]^+$ (100%). ^{1}H NMR δ_H (400 MHz, $CDCl_3$): 9.8 (1H, br, OH), 8.48 (2H, d, J = 5.5 Hz, H^{2,6} Py), 7.60 (2H, d, J = 8.6 Hz, H^{2,6} Ph), 7.55 (2H, d, J = 5.5 Hz, H^{3,5} Py), 6.84 (2H, d, J = 8.6 Hz, H^{3,5} Ph). ^{13}C NMR δ_C (100 MHz, $CDCl_3$): 158.9, 150.3, 147.1, 128.3, 127.8, 120.5, 116.3.

Compound **34B**·HBr·2H_2O. Yield 86%. Found: C, 43.33; H, 4.07; N, 4.61. $C_{11}H_{14}BrNO_4$ requires: C, 43.44; H, 4.46; N, 4.61. *m*/*z* (EI): 215.2 $[M]^+$ (100%). ^{1}H NMR δ_H (400 MHz, $CDCl_3$): 8.38 (2H, dd, J = 1.2, 4.6 Hz, PyH^{2,6}), 7.84 (2H, dd, J = 1.2, 4.6 Hz, PyH^{3,5}), 7.10 (1H, dd, J = 0.2, 8.4 Hz, PhH^6), 7.04 (1H, J = 0.2 Hz, PhH^2), 6.82 (1H, J = 8.4 Hz, PhH^5). ^{13}C NMR δ_C (100 MHz, $CDCl_3$): 156.2, 148.1, 144.4, 140.0, 125.5, 122.2, 121.2, 116.3, 114.6.

Compound **345B**·HBr·0.5H_2O. Yield 98%. Found: C, 44.78; H, 3.92; N, 4.75. $C_{11}H_{11}BrNO_{3.5}$ requires: C, 45.07; H, 3.78; N, 4.78. *m*/*z* (EI): 203.1 $[M]^+$ (100%). ^{1}H NMR δ_H (400 MHz, $CDCl_3$): 8.27 (2H, dd, J = 1.0, 7.0 Hz, PyH^{2,6}), 7.57 (2H, dd, J = 1.0, 7.0 Hz, PyH^{3,5}), 6.44 (2H, s, PhH^{2,6}). ^{13}C NMR δ_C (100 MHz, $CDCl_3$): 144.8, 139.6, 124.2, 121.7, 107.3.

Compounds **4-C*n*** (n = 6, 12, 18), **34-C12**, and **345-C12** were obtained from the corresponding precursors **4B**, **34B**, and **345B** by the synthetic procedure analogous to the preparation of alkylated 5-(alkoxy)picolinaldehydes described by Seredyuk et al.[7b]

Compound **4-C6**. Yield 90%. Found: C, 80.06; H, 8.31; N, 5.43. $C_{17}H_{21}NO$ requires: C, 79.96; H, 8.29; N, 5.49. *m*/*z* (EI): 255.1 $[M]^+$ (100%), 171.0 $[M - C_6H_{13}]^+$ (93%). ^{1}H NMR δ_H (400 MHz, $CDCl_3$): 8.56 (2H, dd, J = 2.0, 5.8 Hz, PyH^{2,6}), 7.55 (2H, dd, J = 1.2, 8.6 Hz, PhH^{2,6}), 7.43 (2H, dd, J = 2.0, 5.8 Hz, PyH^{3,5}), 6.96 (2H, dd, J = 1.2, 8.6 Hz, PhH^{3,5}), 3.97 (2H, t, J = 4.2 Hz, OCH_2), 1.78 (2H, quin, OCH_2CH_2) 1.50−1.25 (6H, m, CH_2), 0.84 (3H, t, J = 4.2 Hz). ^{13}C NMR δ_C (100 MHz, $CDCl_3$): 159.9, 149.8, 147.7, 129.8, 127.9, 120.8, 114.9, 67.9, 31.3, 28.9, 25.5, 22.4, 13.8.

Compound **4-C12**. Yield 92%. Found: C, 81.31; H, 9.81; N, 4.16. $C_{23}H_{33}NO$ requires: C, 81.37; H, 9.80; N, 4.13. *m*/*z* (EI): 339.2 $[M]^+$ (100%), 171.0 $[M - C_{12}H_{25}]^+$ (98%). ^{1}H NMR δ_H (400 MHz, $CDCl_3$): 8.57 (2H, dd, J = 2.0, 5.8 Hz, PyH^{2,6}), 7.54 (2H, dd, J = 1.2, 8.6 Hz, PhH^{2,6}), 7.43 (2H, dd, J = 2.0, 5.8 Hz, PyH^{3,5}), 6.95 (2H, dd, J = 1.2, 8.6 Hz, PhH^{3,5}), 3.97 (2H, t, J = 4.2 Hz, OCH_2), 1.78 (2H, quin, OCH_2CH_2), 1.50−1.20 (18H, m, CH_2), 0.84 (3H, t, J = 4.2 Hz). ^{13}C NMR δ_C (100 MHz, $CDCl_3$): 159.9, 149.9, 147.7, 129.8, 127.9, 120.8, 114.9, 67.9, 31.7, 29.5, 29.4, 29.2, 29.1, 29.0, 25.8, 22.5, 13.9.

Compound **4-C18**. Yield 83%. Found: C, 82.06; H, 10.77; N, 3.21. $C_{29}H_{45}NO$ requires: C, 82.21; H, 10.71; N, 3.31. *m*/*z* (EI): 423.4 $[M]^+$ (46%), 171.0 $[M - C_{18}H_{37}]^+$ (100%). ^{1}H NMR δ_H (400 MHz, $CDCl_3$): 8.57 (2H, dd, J = 2.0, 5.8 Hz, PyH^{2,6}), 7.54 (2H, dd, J = 1.2, 8.6 Hz, PhH^{2,6}), 7.42 (2H, dd, J = 2.0, 5.8 Hz, PyH^{3,5}), 6.95 (2H, dd, J = 1.2, 8.6 Hz, PhH^{3,5}), 3.96 (2H, t, J = 4.2 Hz, OCH_2), 1.77 (2H, quin, OCH_2CH_2) 1.50−1.20 (30H, m, CH_2), 0.84 (3H, t, J = 4.2 Hz). ^{13}C NMR δ_C (100 MHz, $CDCl_3$): 159.9, 149.9, 147.7, 129.8, 127.8, 120.8, 114.8, 67.9, 31.7, 29.5, 29.4, 29.2, 29.0, 25.8, 22.5, 13.9.

Compound **34-C12**. Yield 78%. Found: C, 80.18; H, 10.90; N, 2.60. $C_{35}H_{57}NO_2$ requires: C, 80.25; H, 10.97; N, 2.67. *m*/*z* (EI): 523.7 $[M]^+$ (100%). ^{1}H NMR δ_H (400 MHz, $CDCl_3$): 8.57 (2H, dd, J = 1.2, 4.6 Hz, PyH^{2,6}), 7.43 (2H, dd, J = 1.2, 4.6 Hz, PyH^{3,5}), 7.17 (1H, dd, J = 0.2, 8.4 Hz, PhH^6), 7.10 (1H, J = 0.2 Hz, PhH^2), 6.91 (1H, J = 8.4 Hz, PhH^5), 4.01 (4H, m, OCH_2), 1.80 (4H, quin, J = 4.2 Hz, OCH_2CH_2), 1.46−1.22 (36H, m, CH_2), 0.84 (6H, m, CH_3). ^{13}C NMR δ_C (100 MHz, $CDCl_3$): 150.2, 149.8, 149.3, 147.9, 130.6, 120.9, 119.6, 113.6, 112.5, 69.4, 69.1, 31.7, 29.5, 29.4, 29.2, 29.1, 29.0, 25.8, 22.5, 13.9.

Compound **345-C12**. Yield 60%. Found: C, 79.78; H, 11.40; N, 2.11. $C_{47}H_{81}NO_3$ requires: C, 79.72; H, 11.53; N, 1.98. *m*/*z* (EI): 707.4 $[M]^+$ (70%). ^{1}H NMR δ_H (400 MHz, $CDCl_3$): 8.65 (2H, dd, J = 1.0, 6.1 Hz, PyH^{2,6}), 7.48 (2H, dd, J = 1.0, 6.1 Hz, PyH^{3,5}), 6.82 (2H, s, PhH^{2,6}), 4.06 (6H, m, OCH_2), 1.85 (6H, m, OCH_2CH_2), 1.53−1.28 (54H, m, CH_2), 0.90 (9H, m, CH_3). ^{13}C NMR δ_C (100 MHz, $CDCl_3$): 153.5, 149.8, 148.4, 139.2, 133.0, 121.3, 105.6, 73.4, 69.2, 31.7, 30.1, 29.5−29.2, 25.9, 22.5, 13.9.

General Synthetic Procedure for Compounds 1−22. To a hot solution of an alkylated ligand (1.22 mmol) and $FeCl_2 \cdot 2H_2O$ (0.10 g, 0.61 mmol) in hot ethanol was added dropwise a solution of $[N(t\text{-}Bu)_4]_2[M^{II}(CN)_4]$ (M^{II} = Ni, Pd, Pt) (0.61 mmol) or $[N(t\text{-}Bu)_4][M^{I}(CN)_2]$ (M^{I} = Ag, Au) (1.22 mmol) in ethanol, which was immediately accompanied by the formation of a precipitate. The mixture was stirred for 15 min and then centrifuged. After that, the solution was decanted and the rest washed with ethanol and centrifuged. The precipitate was dried in vacuo.

Compound **1**. **4-C6** (0.31 g), $[N(t\text{-}Bu)_4]_2[Ni(CN)_4]$ (0.28 g). $C_{38}H_{44}FeN_6NiO_3$ requires: C, 61.07; H, 5.93; N, 11.25. Found: C, 61.42; H, 5.63; N, 11.26

(11) Gessner, W.; Brossi, A.; Rong-sen, S.; Abell, C. W. *J. Med. Chem.* **1985**, *28*, 311.

Compound **2**. **4-C18** (0.52 g), $[N(t\text{-}Bu)_4]_2[Ni(CN)_4]$ (0.28 g). $C_{55}H_{77}FeN_6NiO_3$ requires: C, 68.70; H, 8.55; N, 7.75. Found: C, 68.85; H, 8.89; N, 7.69

Compound **3**. **4-C12** (0.41 g), $[N(t\text{-}Bu)_4]_2[Ni(CN)_4]$ (0.28 g). $C_{50}H_{67}FeN_6NiO_{2,5}$ requires: C, 66.24; H, 7.45; N, 9.27. Found: C, 66.68; H, 7.42; N, 8.78

Compound **4**. **34-C12** (0.64 g), $[N(t\text{-}Bu)_4]_2[Ni(CN)_4]$ (0.28 g). $C_{74}H_{118}FeN_6NiO_6$ requires: C, 68.25; H, 9.13; N, 6.45. Found: C, 68.56; H, 9.06; N, 6.45

Compound **5**. **345-C12** (0.87 g), $[N(t\text{-}Bu)_4]_2[Ni(CN)_4]$ (0.28 g). $C_{97}H_{163}FeN_6NiO_8$ requires: C, 70.36; H, 9.92; N, 5.08. Found: C, 69.84; H, 9.62; N, 4.97

Compound **6**. **4-C18** (0.52 g), $[N(t\text{-}Bu)_4]_2[Pd(CN)_4]$ (0.42 g). $C_{55}H_{77}FeN_6O_3Pd$ requires: C, 63.98; H, 7.52; N, 8.14. Found: C, 64.02; H, 7.55; N, 8.48

Compound **7**. **4-C12** (0.41 g), $[N(t\text{-}Bu)_4]_2[Pd(CN)_4]$ (0.42 g). $C_{49}H_{65}FeN_6O_3Pd$ requires: C, 62.06; H, 6.91; N, 8.86. Found: C, 62.40; H, 7.02; N, 8.48

Compound **8**. **34-C12** (0.64 g), $[N(t\text{-}Bu)_4]_2[Pd(CN)_4]$ (0.42 g). $C_{74}H_{115}FeN_6O_{4,5}Pd$ requires: C, 67.18; H, 8.76; N, 6.35. Found: C, 67.67; H, 8.43; N, 6.07

Compound **9**. **345-C12** (0.87 g), $[N(t\text{-}Bu)_4]_2[Pd(CN)_4]$ (0.42 g). $C_{97}H_{165}FeN_6O_9Pd$ requires: C, 67.67; H, 9.66; N, 4.88. Found: C, 67.51; H, 9.29; N, 5.10

Compound **10**. **4-C18** (0.52 g), $[N(t\text{-}Bu)_4]_2[Pt(CN)_4]$ (0.48 g). $C_{55}H_{77}FeN_6O_3Pt$ requires: C, 58.92, H, 6.92, N, 7.50. Found: C, 58.84, H, 6.53, N, 7.64

Compound **11**. **4-C12** (0.41 g), $[N(t\text{-}Bu)_4]_2[Pt(CN)_4]$ (0.48 g). $C_{49}H_{65}FeN_6O_3Pt$ requires: C, 56.75; H, 6.32; N, 8.10. Found: C, 57.16; H, 6.46; N, 7.94

Compound **12**. **34-C12** (0.64 g), $[N(t\text{-}Bu)_4]_2[Pt(CN)_4]$ (0.48 g). $C_{74}H_{116}FeN_6O_5Pt$ requires: C, 62.56; H, 8.23; N, 5.92. Found: C, 62.25; H, 7.79; N, 6.31

Compound **13**. **345-C12** (0.87 g), $[N(t\text{-}Bu)_4]_2[Pt(CN)_4]$ (0.48 g). $C_{97}H_{163}FeN_6O_8Pt$ requires: C, 65.00; H, 9.17; N, 4.69. Found: C, 65.46; H, 9.12; N, 4.74

Compound **14**. **4-C18** (0.52 g), $[N(t\text{-}Bu)_4][Ag(CN)_2]$ (0.49 g). $C_{91}H_{136}Ag_2FeN_7O_{3,5}$ requires: C, 66.01; H, 8.28; N, 5.92. Found: C, 66.03; H, 8.60; N, 6.16

Compound **15**. **4-C12** (0.41 g), $[N(t\text{-}Bu)_4][Ag(CN)_2]$ (0.49 g). $C_{73}H_{100}Ag_2FeN_7O_{3,5}$ requires: C, 62.48; H, 7.18; N, 6.99. Found: C, 62.24; H, 7.15; N, 6.92

Compound **16**. **34-C12** (0.64 g), $[N(t\text{-}Bu)_4][Ag(CN)_2]$ (0.49 g). $C_{107}H_{167}Ag_2FeN_7O_7$ requires: C, 66.41; H, 8.70; N, 5.07. Found: C, 66.76, H, 8.72, N, 5.03

Compound **17**. **345-C12** (0.87 g), $[N(t\text{-}Bu)_4][Ag(CN)_2]$ (0.49 g). $C_{143}H_{241}Ag_2FeN_7O_{11}$ requires: C, 68.53; H, 9.69; N, 3.91. Found: C, 68.36; H, 9.79; N, 3.62

Compound **18**. **4-C6** (0.31 g), $[N(t\text{-}Bu)_4][Au(CN)_2]$ (0.60 g). $C_{55}H_{65}Au_2FeN_7O_4$ requires: C, 49.37; H, 4.90; N, 7.33. Found: C, 49.41; H, 4.97; N, 7.43

Compound **19**. **4-C18** (0.52 g), $[N(t\text{-}Bu)_4][Au(CN)_2]$ (0.60 g). $C_{91}H_{136}Au_2FeN_7O_{3,5}$ requires: C, 59.60; H, 7.47; N, 5.35. Found: C, 59.21; H, 7.31; N, 4.93

Compound **20**. **4-C12** (0.41 g), $[N(t\text{-}Bu)_4][Au(CN)_2]$ (0.60 g). $C_{73}H_{99}Au_2FeN_7O_3$ requires: C, 55.76, H, 6.35, N, 6.24. Found: C, 56.17, H, 5.98, N, 6.53

Compound **21**. **34-C12** (0.64 g), $[N(t\text{-}Bu)_4][Au(CN)_2]$ (0.60 g). $C_{73}H_{115}Ag_2FeN_6O_6$ requires: C, 60.71; H, 8.03; N, 5.82. Found: C, 60.89; H, 8.52; N, 5.59

Compound **22**. **345-C12** (0.87 g), $[N(t\text{-}Bu)_4][Au(CN)_2]$ (0.60 g). $C_{143}H_{238}Au_2FeN_7O_{9,5}$ requires: C, 64.64; H, 9.03; N, 3.69. Found: C, 64.54; H, 9.09; N, 3.60

Physical Characterization. The iron *K*-edge X-ray absorption near-edge structures (XANES) and extended X-ray absorption fine structures (EXAFS) spectra were recorded in the conventional transmission mode on beamline A1 at the German Electron Synchrotron, DESY, Hamburg. The spectrum was recorded from 6970 to 7997 eV. The energy scale at the iron *K* edge was calibrated with the strong absorption peak of metallic iron foil at 7111.2 eV. A water-cooled Si(111) channel-cut crystal was used as a monochromator. The intensities of the incident and transmitted X-rays were recorded using ionization chambers. The mass of the sample was calculated to obtain a product $a \times d$ of about 2.5 for energies just above the absorption *K* edge of iron (a is the linear absorption coefficient, and d is the thickness of the pellet). The calculated amount of the sample was ground, mixed with crystalline cellulose, and pressed into a 13-mm-diameter and about 1-mm-thick pellet. A closed-cycle He cryostat was used for variable temperature measurements. The temperature was measured with a Si diode placed close to the sample. The data acquisition time for each data point was 1 s. EXAFS data analysis was performed with the program *EXAFS98*.[12a,b] This standard analysis includes linear pre-edge background removal, a Lengeler−Eisenberg spectrum normalization, and reduction from the absorption data $\mu(E)$ to the EXAFS spectrum $\chi(k)$ with

$$k = \sqrt{\frac{2m_\varepsilon}{(\hbar)^2}(E - E_0)}$$

where E_0 is the energy threshold, taken at the absorption maximum (7130 ± 1 eV). The radial distribution function $F(R)$ was calculated by Fourier transformation of $k^3\, w(k)\, \chi(k)$ in the 2−14 $Å^{-1}$ range; $w(k)$ is a Kaiser−Bessel apodization window with smoothness coefficient $\tau = 3$. After Fourier filtering, the first single shell Fe−N_6 was fitted in the 4−12 $Å^{-1}$ range to the standard EXAFS formula, in a single scattering scheme:

$$k_\chi(k) = -S_0^2 \sum_{i=1.5} \left[\frac{N_i}{R_2^i} |(F\pi, k)| e^{-2\sigma^2 k^2}\, e^{-2Ri/\lambda(k)} \sin(2kR_i + 2\partial_1(k) + \Psi(k)) \right]$$

where S_0^2 is the inelastic reduction factor, N is the number of nitrogen atoms at distance R from the iron center, $\lambda(k)$ is the mean free path of the photoelectron, σ is the Debye−Waller factor, giving the width of the Fe−N distance distribution, $\partial_1(k)$ is the central atom phase shift, and $|(F\pi,k)|$ and $\psi(k)$ are the amplitude and phase of the nitrogen backscattered wave. The curve-fitting analysis for the first coordination sphere of the iron was performed with the *Round Midnight*[12c] code after Fourier filtering in the 0.7−2.0 Å range of the EXAFS spectrum. Spherical-wave theoretical amplitudes and phase shifts calculated by the *McKale*[12d,e] code were used. Since theoretical phase shifts were used, we fitted the energy threshold E_0 (ΔE_0). The goodness of fit was given by

$$\rho(\%) = \frac{\sum [k\chi_{\mathrm{exp}}(k) - k\chi_{\mathrm{th}}(k)]^2}{\sum [k\chi_{\mathrm{exp}}(k)]^2}$$

Variable-temperature magnetic susceptibility measurements of samples **1**−**22** (20−30 mg) were recorded with a Quantum Design MPMS2 SQUID susceptometer equipped with a 7 T magnet, operating at 1 T and at temperatures from 1.8−400 K. The susceptometer was calibrated with $(NH_4)_2Mn(SO_4)_2 \cdot 12H_2O$. Experimental susceptibilities were corrected for diamagnetism of the constituent atoms by the use of Pascal's constants. Mössbauer spectra were recorded in transmission geometry with a ^{57}Co/Rh source kept at room temperature and a conventional spectrometer operating in the constant-acceleration mode. The samples were sealed in a Plexiglas sample holder and mounted in a nitrogen-bath cryostat. The Recoil 1.03a Mössbauer Analysis Software (Dr. E. Lagarec; http://www.isapps.ca/recoil/) was used to fit the experimental spectra.

DSC measurements were performed on a Mettler model DSC 822e calibrated with metallic indium and zinc. An overall accuracy of 0.2 K was estimated in the temperature control and 2% in the heat flow. DSC profiles were recorded at the rate

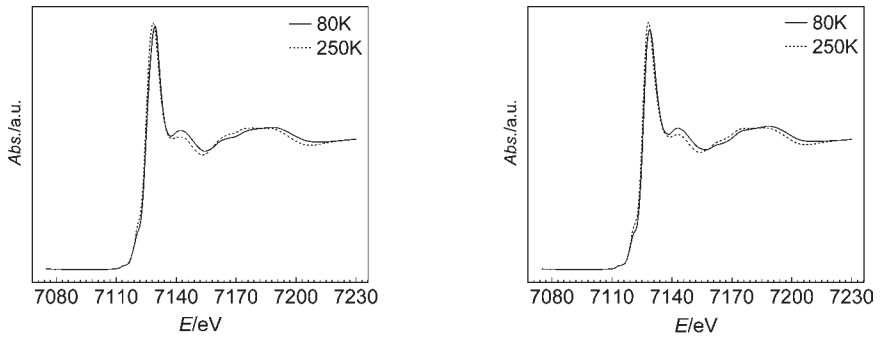

Figure 1. Normalized XANES spectra of compounds **2** and **6**.

of 10 K/min and analyzed with Netzsch Proteus software (NETZSCH-Geraetebau GMBH, http://www.e-thermal.com/proteus.htm).

High-resolution powder diffraction patterns were collected in the Debye−Scherrer mode on the high-resolution powder diffractometer at ID31 of the European Synchrotron Radiation Facility (ESRF, Grenoble) coupled with a liquid nitrogen cryostat. The samples were sealed in lithium borate glass capillaries of diameter 0.5 mm (Hilgenberg glass No. 50) and rotated around θ in order to improve the spatial averaging. The exact wavelength and the zero point were determined from well-defined reflections of a silicon standard ($\lambda = 0.29941892 \pm 0.00009008$ Å). At ID31, nine crystal analyzers [nine Ge(111) crystals separated by 2° intervals] with nine Na(Tl)I scintillation counters were used simultaneously. The incoming beam was monitored using an ion chamber for normalization purposes in order to take the decay of the primary beam into account.

IR spectra were recorded at 293 K using a Bruker Tensor 27 Spectrometer in the range of 400−4000 cm^{-1}. Elemental analyses were done on a Vario EL Mikro Elementanalysator. TGA measurements were performed on a Mettler Toledo TGA/SDTA 851, in the 300−680 K temperature range in a nitrogen atmosphere with a rate of 10 K/min. Microanalysis was done by using PV 9760 EDAX Microanalysis with a PHILIPS XL 30 ESEM scanning electron microscope.

Results and Discussion

X-Ray Absorption Spectroscopy (XAS and EXAFS). Structural Characterization of 2 and 6. In the family of Hofmann-like polymers of iron(II) with monodentate ligands, the X-ray single-crystal structure is known for {Fe(py)$_2$[Ni(CN)$_4$]} and related compounds,[13] whereas EXAFS characterization of the {Fe(4-PhPy)$_2$[M^{II}(CN)$_4$]}·sH$_2$O compounds was reported by us recently.[9] The fragment of the 2D polymeric structure sketched in Scheme 1 consists of iron(II) ions surrounded by pyridine moieties and bridging tetracyanidenickelate anions. Since it is impossible to obtain single crystals of compounds **1**−**22** suitable for X-ray diffraction, we have used extended X-ray absorption fine structure (EXAFS) spectroscopy for their structural characterization.

Figure 1 shows the normalized edge spectra of complexes **2** and **6** at different temperatures. In both complexes, the energy of the *K* edge is shifted to lower energy on heating the sample, demonstrating the increased Fe−N distances associated with the LS to HS spin transition. The radial distributions for **2** and **6** at low and high temperatures are presented in Figure 2. The first shell (I) is formed by nitrogen atoms which belong to bridging tetracyanide groups in the equatorial plane and to axial pyridine molecules or oxygen atoms of water molecules. The second shell (II) includes carbon atoms of cyanide groups and of pyridine molecules. The third one (III) is essentially due to heavy Ni/Pd atoms of the $[Ni(CN)_4]^{2-}$/$[Pd(CN)_4]^{2-}$ groups. Using a simple scattering model, we could analyze quantitatively the first shell of neighbors I, which reflects the structural changes accompanying the spin transition (Table 1). The fitted bond distances for the first FeN_6 coordination shell compare well with those of related iron(II) polymers in both spin states.[9] For **2**, XAS was used to explore changes at the iron *K* edge at different temperatures and at the nickel *K* edge at 250 K. Both sets of data show similar patterns with three dominant peaks attributed to the first three coordination shells (Figure 3). Like in the previously reported parent Ni compound,[9] peak III at the iron *K* edge is more intense than at the nickel *K* edge. On the other hand, peak II at the iron *K* edge is less intense than the one at the nickel *K* edge (V). This is essentially similar to previously reported observations[9] and indicates a slight tilt of the $[Ni(CN)_4]^{2-}$ groups such that the angle Fe−C−N deviates from 180° while the Ni−C−N angle is perfectly aligned.[13a] This fact leads to a focusing effect on N in the case of the nickel *K* edge experiment and low intensity of the Fe peak in the case of the Fe *K* edge experiment (Figure 3). On the other hand, at the Fe *K* edge, the focusing effect on Ni through the carbon atom intensifies the signal of Ni in the Fourier transform but not on the C (peak II is much less intense than peak V). At the Ni *K* edge, the peaks in the Fourier transform are assigned to four carbon atoms of cyanide ligands (mean distance = 1.88 Å) for the first shell, to the cyanide nitrogen atoms for the second shell, and to Fe atoms for the third shell, visible at *ca.* 4.7 Å. The analysis of the Ni−C shell is given in Table 2.

At the Fe *K* edge, **6** has the same first coordination shell as **2** (six nitrogen neighbors, Fe−N distance is 1.96 Å in the LS state and *ca.* 2.16 Å in the HS state, see Table 1) and the same second shell consisting of carbon atoms of CN groups and pyridines. The third shell of the heavy Pd atom appears at about 4.8 Å. The significant intensity of

(12) (a) Michalowicz, A. EXAFS98 pour la Mac. In *Logiciels pour la Chimie*; Société Française de Chimie: Paris, 1991; p 102. (b) Michalowicz, A. *J. Phys. IV France* **1997**, *7*, 235. (c) Michalowicz, A. Round Midnight. In *Logiciels pour la Chimie*; Société Française de Chimie: Paris, 1991; p 116. (d) McKale, A. G.; Knapp, G. S.; Chan, S. K. *Phys. Rev. B* **1986**, *33*, 841. (e) McKale, A. G.; Veal, B. W.; Paulikas, A. P.; Chan, S.-K.; Knapp, G. S. *J. Am. Chem. Soc.* **1988**, *110*, 3763–3768.

(13) (a) Kitazawa, T.; Gomi, Y.; Takahashi, M.; Takeda, M.; Enomoto, M.; Miyazaki, A.; Enoki, T. *J. Mater. Chem.* **1996**, *6*, 119. (b) Kitazawa, T.; Eguchi, M.; Takeda, M. *Mol. Cryst. Liq. Cryst.* **2000**, *341*, 1331. (c) Real, J. A.; Gaspar, A. B.; Muñoz, M. C. *Dalton Trans.* **2005**, 2062.

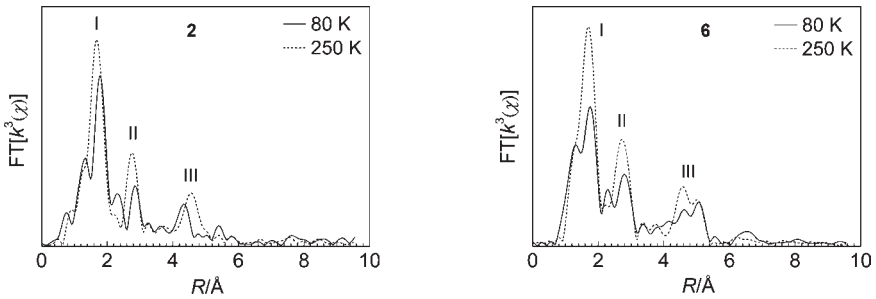

Figure 2. Fourier transforms of the iron *K*-edge EXAFS signal for **2** and **6** at low and high temperatures. I, II, and III correspond to Fe−N, Fe−C, and Fe−M (M = Ni or Pd) distances, respectively.

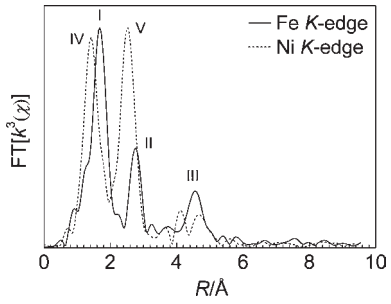

Figure 3. Comparison of Fourier transforms of the EXAFS spectra at Ni and Fe *K* edges of complex **2** at 250 K.

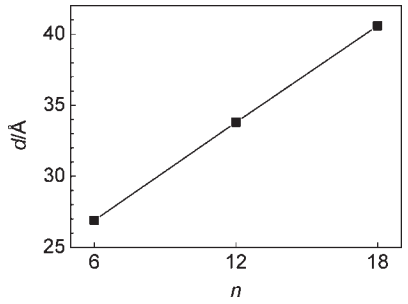

Figure 4. Dependence of the interlayer distance *d* on the length of single alkyl substituents in **1**−**3**−**2**.

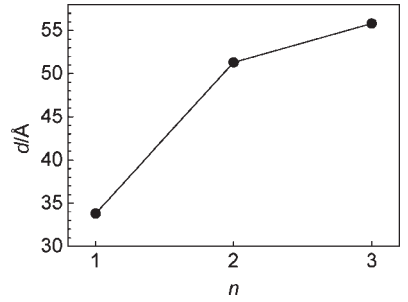

Figure 5. Dependence of the intrerlayer distance *d* on the number of ligand substituents with increasing number of alkyl chains in **3**−**4**−**5**.

Table 1. Best Fit for Structural Parameters of the First Coordination Shell (I) of **2** and **6**

compound	T/K	N^{HS}	N^{LS}	R^{HS}/Å	R^{LS}/Å	σ^{HS}/Å	σ^{LS}/Å	ΔE/eV	ρ/%
2	80	4.8	1.2	2.16	1.95	0.088	0.065	−1.3	8.8
	250	5.8	0.2	2.18	1.95	0.088	0.065	−0.3	7.9
6	80	4.7	1.3	2.15	1.96	0.088	0.065	−0.3	6.0
	250	6.0		2.17		0.088		1.7	3.2

the last peak is due to the focusing effect on linear cyanide bridges.[14]

X-Ray Powder Diffraction (XRPD) for 1−22. The XRPD patterns of compounds **1**−**22** were measured at 300 K (SFigure 1, Supporting Information). The patterns of derivatives **1** and **3** with C6 and C12 single alkyl chains, respectively, are of poor quality, reflecting the low crystallinity of the samples. Lengthening of alkyl substituents leads to resolution of the peaks ascribed to the (10), (20), (30), and (40) reflections, revealing a well-defined layered structure in **2**. In the diffractogram, high order reflections disappear with an increasing number of substituents up to two and three; however, the intensity of the alkyl halo increases. In the patterns of all compounds, peaks at $2\theta \approx$ 17.5 and 25.0° are also observed with corresponding *d* spacings of 5.10 and 3.55 Å, respectively, originating from a face-centered monomeric unit of the Fe−M polycyanide array in the HS state (Table 3). Similar patterns have been previously observed for Prussian blue thin films.[15]

A comparison of the interlayer distances in derivatives **1**, **3**, and **2** with C6, C12, and C18 single alkyl chains, respectively, shows a linear increase of the interlayer distance by 1.14 Å per methylen group, which corresponds to a tilt angle of alkyl chains equal to 26.1° (Figure 4). In the series **3**−**4**−**5** with one, two, and three C12-alkyl chains per ligand molecule, respectively, the simple dependence of the interlayer distance on the number of alkyl substituents is not observed (Figure 5). Since the chemical analysis does not reveal a deviation of the composition from the expected one, we can anticipate that in all compounds the Fe(II) ions are coordinated by cyano groups and ligand molecules, except

Table 2. Best Fit for Structural Parameters of the First Coordination Shell (V) of **2** at 250 K

N	R^C/Å	σ^C/Å	ΔE/eV	ρ/%
4	1.88	0.057	−0.15	2.2

Table 3. Interlayer Distances *d* for **1**−**22**

subst.	*d*/Å	subst.	*d*/Å	subst.	*d*/Å	subst.	*d*/Å	subst.	*d*/Å
1	26.9							**18**	19.9
2	40.6	**6**	42.4	**10**	42.0	**14**	30.4	**19**	30.0
3	33.8	**7**	34.6	**11**	33.5	**15**	25.4	**20**	24.2
4	51.3	**8**	49.0	**12**	49.6	**16**	31.2	**21**	24.5
5	55.8	**9**	54.4	**13**	53.7	**17**	36.9	**22**	37.2

(14) Yokoyama, T.; Murakami, Y.; Kiguchi, M.; Komatsu, T.; Kojima, N. *Phys. Rev. B: Condens. Matter* **1998**, *58*, 14238.
(15) Yamamoto, T.; Umemura, Y.; Sato, O.; Einaga, Y. *J. Am. Chem. Soc.* **2005**, *127*, 16065.

Table 4. The Stretching Frequencies ν(CN) in **1**−**22**

subst.	ν/cm^{-1}	subst.	ν/cm^{-1}	subst.	ν/cm^{-1}	subst.	ν/cm^{-1}	subst.	ν/cm^{-1}
1	2172							**18**	2172
2	2150	**6**	2167	**10**	2165	**14**	2161, 2063	**19**	2171
3	2154	**7**	2166	**11**	2166	**15**	2168, 2069	**20**	2172
4	2155	**8**	2170	**12**	2168	**16**	2164, 2075	**21**	2172
5	2168	**9**	2168	**13**	2166	**17**	2165, 2078	**22**	2170

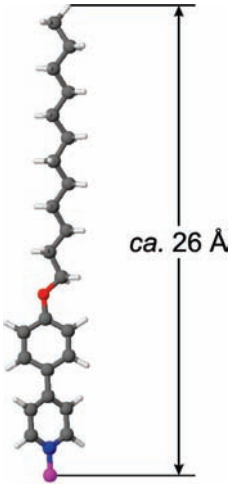

Figure 6. The total maximal length of the bond Fe−N and the stretched ligand 4(4-dodecyloxyphenyl)pyridine with the alkyl chain in all-*trans* configuration.

terminal sites. Comparing the cross sections of a monomeric unit (51 Å^2, from X-ray data of $\{Fe(py)_2[Ni(CN)_4]\}$[13a]) and of two all-*trans* alkyl chains of the ligand 34-C12 (18 × 2 = 36 Å^2) or three alkyl chains of the ligand 345-C12 (18 × 3 = 54 Å^2), we assume that in the second case the alkyl chains must be perpendicular to the plane formed by the polycyanide framework.[16] Indeed, the theoretically estimated sum of lengths of two ligand molecules 4-C12 (also 34-C12 and 345-C12) in the stretched form (Figure 6) together with the two bond lengths Fe−N is equal to *ca.* 52 Å, and this is in a good agreement with the experimentally found *d* values (see Table 3). In the case of **4**, the difference in relative cross-sectional areas occupied by the alkyl chains and a monomeric unit of the polymeric framework is compensated by a chain axis tilt with an estimated angle equal to 10.6°.

From the analysis of the XRPD data, one can conclude that a common structural feature among all homologues of the series is a similar layered structure, and adoption on melting of a smectic mesophase at ca. 350−375 K.

IR Spectroscopy and EDXA Data. The formation of Fe−N≡C−M bridges in polynuclear complexes **1**−**22** is evidenced by the stretching vibrations of the cyanide ligands. The IR data are summarized in Table 4. The ν(CN) modes are shifted to higher frequencies analogously to the parent compounds, confirming the formation of the polymeric heterometallic structures.[17] In the spectra of the $[Ag(CN)_2]^-$-based compounds, two CN bands are observed which differ by about 100 cm^{-1}. This fact and the ratio Fe/L = 1:3 deduced from the CHN analysis data point at the presence of bridging anions $[Ag(CN)_2]^-$ and $[Ag(L)(CN)_2]^-$ with three-coordinated silver atoms, analogously to the structurally characterized 3-bromo- and 3-iodopyridine-based complexes described by Muñoz et al.[18] and pyridine complexes of $[Ag(CN)_2]^-$.[19] Accordingly, the higher frequency of the ν(CN) band is assigned to the CN groups bonded to double coordinate Ag atoms without an attached pyridine molecule. The second band is assigned to the $[Ag(CN)_2]^-$ groups where each triply coordinate Ag atom bears a ligand molecule. Expectedly, in the IR spectra of the $[Au(CN)_2]^-$-based complexes, the splitting of the CN band is not observed, reflecting the absence of bonding between ligand molecules and dicyanoaurate groups.

A confirmation that formed networks are heterometallic is also found by EDXA spectroscopy (energy-dispersive X-ray microanalysis). A scan of powdered samples shows both Fe and M peaks. The quantitative analysis of the integrated areas of the multiplex scans yields an Fe/M ratio of 1:1 ± 5% (M^{II} = Pd, Ni, or Pt) or 1:2 ± 5% (M^{I} = Ag or Au).

Magnetic Susceptibility Measurements. The thermal dependence of the product $\chi_M T$ (χ_M being the molar susceptibility and T the temperature) for compounds **1**−**22** is displayed in Figure 7. The temperature dependence of the magnetic susceptibility was recorded at a rate of 2 K min^{-1}. The $\chi_M T$ value for all compounds at room temperature is near 3.50 cm^3 K mol^{-1}, which reveals the HS configuration of Fe(II) ions. In all compounds except for $[Ag(CN)_2]^-$ derivatives, an incomplete gradual HS↔LS transition with $T_{1/2} \approx 170$ K is observed accompanied by a pronounced change of color [from yellow (HS) to red (LS)]. This feature is indicative of weakly cooperative character of the transition, contrary to the parent compounds where abrupt transitions with hysteresis up to 40 K were found.[9] An explanation for the observed behavior could be the absence of appreciable interactions between Fe centers, whereas in the parent compounds it is mediated by strong $\pi-\pi$ interactions between pyridine and phenyl rings of the ligand molecules.[9] In all compounds, the decrease of the susceptibility below 30 K is due to the zero field splitting of the Fe(II) ions with the ground state $S = 2$.[20]

The magnetic behavior of the silver derivatives is unique in the series. While in the majority of the compounds, *ca.* 50% of Fe(II) ions undergo transition to the LS state, in the Ag compounds, this value is nearly 10%. The explanation must be looked for in the bonding of an additional ligand molecule to the bridging $[Ag(CN)_2]^-$ groups, which can substantially change the strength of the ligand field at the Fe(II) center and insert sterical hindrance for the transformation of the HS polymeric layer to a more compact one with LS Fe(II) ions.

(16) Dorset, D. L. *Crystallography of the polymethylene chain: an inquiry into the structure of waxes*: Oxford University Press: Oxford, U. K., 2005.
(17) (a) Zhan, S.-z.; Guo, D.; Zhang, X.-y.; Du, C.-x.; Zhu, Y.; Yang, R.-n. *Inorg. Chim. Acta* **2000**, *298*, 57. (b) Nakamoto, K. *Infrared and Raman spectra of inorganic and coordination compounds*; John Wiley: New York, 1986.
(18) Munoz, M. C.; Gaspar, A. B.; Galet, A.; Real, J. A. *Inorg. Chem.* **2007**, *46*, 8182.
(19) Bowmaker, G. A.; Junk, P. C.; Skelton, B. W.; White, A. H. *Z. Naturforsch., B: Chem. Sci.* **2004**, *59*, 1277.
(20) Carlin, L. R. *Magnetochemistry*; Springer: Berlin, 1986.

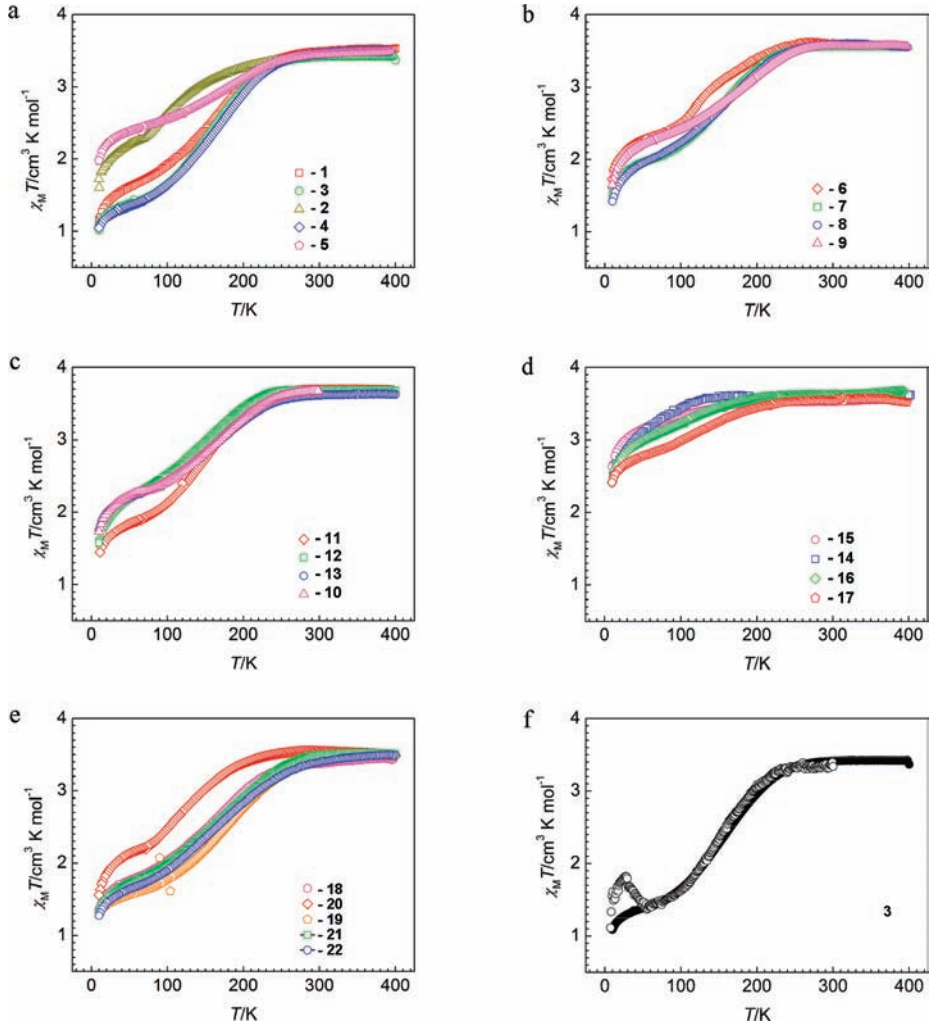

Figure 7. Thermal variation of the $\chi_M T$ product from magnetic measurements of compounds **1**−**22** (a−e). LIESST effect upon irradiation at 4 K with subsequent increase in temperature for compound **3** (f).

Irradiation of the pristine compound **3** at 4 K with a green laser (λ = 514 nm) causes partial photoconversion of the LS molecules into a metastable HS state. As an example, in Figure 7f, the LIESST effect[21] is shown for complex **3**, where the critical temperature of relaxation T^{LIESST} is 40 K.

The heating of the compounds up to 400 K and subsequent cooling do not reveal any considerable changes in their magnetic behavior due to melting or dehydration.

Mössbauer Spectroscopy Data. The temperature dependence of the ^{57}Fe Mössbauer spectra of **1**−**13** has been studied in the low- and high-temperature regions. Values of the Mössbauer parameters from a least-squares fit are listed in Table 5. The variation of the molar fractions, A, compares well with the data deduced from the magnetic susceptibility measurements. A representative spectrum of **3** (Figure 8) and of **1**, **2**, and **4**−**13** (SFigure 3, Supporting Information) at 80 K consists of one LS and three HS doublets. The HS doublets are most probably related to the presence of terminal Fe(II) sites in relatively small polymeric particles. In this case, a coordination polyhedron of the type $[FeN_{6-x}O_x]$ must be realized which favors the HS configuration of the Fe(II) ion in the whole temperature range. The size of the quadrupole splitting reflects the extent of structural distortion of the $[FeN_{6-x}O_x]$ chromophor. The electric field gradient (EFG) determining the size of the quadrupole splitting is the sum of two contributions. One arises from noncubic valence electron distribution at the SCO iron center and is denoted as $(EFG)_{val}$. The other one, denoted as $(EFG)_{lat}$, arises from structural distortions within the $[FeN_{6-x}O_x]$ chromophor and/or substitution of nitrogen atoms by O atoms of coordinated water molecules, both effects leading to symmetry lowering to lower than cubic. As the two contributions to the total EFG have opposite signs, the observed quadrupole splitting ΔE_Q is small (large) in the case of large (small) $(EFG)_{lat}$.

The Au-containing compounds (**18**−**22**) have also been characterized by Mössbauer spectroscopy. The spectra, however, showed poor resolution in nearly all cases due to an insufficient signal-to-noise ratio because of strong K-edge absorption in gold atoms, which weakens the 14.4 keV Mössbauer γ radiation. Nevertheless, a qualitative analysis of the spectra was possible. The area fractions of the HS and LS resonance signals estimated from the spectra matched well the results from the magnetic measurements.

(21) (a) Decurtins, S.; Gütlich, P.; Köhler, C. P.; Spiering, H.; Hauser, A. *Chem. Phys. Lett.* **1984**, *105*, 1. (b) Lètard, J.-F. *J. Mat. Chem.* **2006**, *16*, 2550.

Table 5. Least-Squares-Fitted ^{57}Fe Mössbauer Spectra for **1**−**13**[a]

compound	T/K	doublet	ΔE_q/mm s^{-1}	δ/mm s^{-1}	$\Gamma_{1/2}$/mm s^{-1}	A/%
1	80	LS	0.485(15)	0.225(33)	0.195(28)	51.9(36)
		HS1	1.058(71)	1.54(16)	*0.2*	13.6(40)
		HS2	1.141(28)	2.162(79)	*0.2*	25.2(46)
		HS3	1.101(68)	2.80(17)	*0.2*	9.3(38)
2	85	LS	0.457(25)	0.253(38)	*0.2*	23.52(96)
		HS1	1.1686(69)	1.264(14)	*0.2*	73.2(13)
		HS2	1.162(74)	2.95(15)	*0.2*	3.3(10)
3	80	LS	0.4567(83)	0.23(10)	*0.2*	68.31(79)
		HS1	1.248(24)	1.35(10)	*0.2*	14.9(19)
		HS2	1.273(33)	1.86(11)	*0.2*	10.9(19)
		HS3	1.239(32)	2.93(21)	*0.2*	5.97(80)
4	80	LS	0.5(14)	0.3(28)	*0.2*	68.8(12)
		HS1	1.1(66)	2(13)	*0.2*	14.4(33)
		HS2	1.181(42)	2.04(11)	*0.2*	10.2(33)
		HS3	1.164(45)	2.865(99)	*0.2*	6.6(14)
5	80	LS	0.4696(75)	0.2312(97)	*0.2*	33.38(55)
		HS1	1.1893(77)	1.455(15)	*0.2*	24.76(97)
		HS2	1.1733(69)	2.167(21)	*0.2*	20.82(97)
		HS3	1.1380(63)	2.836(15)	*0.2*	21.04(75)
6	80	LS	0.4965(82)	0.24(1)	0.17(1)	39.1(12)
		HS1	1.158(15)	1.34(6)	0.20(5)	22.0(10)
		HS2	1.192(18)	1.96(9)	0.25(1)	24.0(16)
		HS3	1.178(22)	2.90(10)	0.273(65)	15.7(68)
7	80	LS	0.5064(48)	0.2128(62)	0.1751(55)	46.72(65)
		HS1	1.154(12)	1.24(4)	0.190(35)	15.7(63)
		HS2	1.1693(84)	1.76(5)	0.248(33)	29.9(79)
		HS3	1.138(19)	2.93(6)	0.246(46)	7.7(19)
8	80	LS	0.4799(61)	0.2492(81)	*0.2*	49.02(45)
		HS1	1.1985(83)	1.316(20)	*0.2*	22.85(96)
		HS2	1.230(12)	1.878(23)	*0.2*	17.29(96)
		HS3	1.2076(97)	2.984(20)	*0.2*	10.83(43)
9	80	LS	0.4696(75)	0.2312(97)	*0.2*	33.38(55)
		HS1	1.1893(77)	1.455(15)	*0.2*	24.76(97)
		HS2	1.1733(69)	2.167(21)	*0.2*	20.82(97)
		HS3	1.1380(63)	2.836(15)	*0.2*	21.04(75)
10	85	LS	0.527(17)	0.155(55)	*0.2*	42.5(26)
		HS1	1.06(49)	1.49(98)	*0.2*	15.4(44)
		HS2	1.23(24)	1.87(48)	*0.2*	30.3(44)
		HS3	1.282(51)	3.04(10)	*0.2*	11.8(25)
11	80	LS	0.50(2)	0.20(4)	*0.2*	57.6(29)
		HS1	1.30(7)	2.00(1)	*0.2*	15.9(46)
		HS2	1.18(1)	1.15(2)	*0.2*	14.3(44)
		HS3	1.22(5)	2.77(1)	*0.2*	12.2(28)
12	80	LS	0.485(22)	0.244(28)	*0.2*	49.2(26)
		HS1	1.177(44)	2.21(11)	*0.2*	15.4(34)
		HS2	1.178(37)	1.373(74)	*0.2*	21.5(37)
		HS3	1.234(44)	3.102(93)	*0.2*	13.9(27)
13	80	LS	0.516(13)	0.148(46)	*0.2*	38.5(17)
		HS1	1.120(26)	1.501(61)	*0.2*	26.1(26)
		HS2	1.145(24)	2.193(66)	*0.2*	19.0(25)
		HS3	1.138(25)	2.899(59)	*0.2*	16.4(22)

[a] The values given in italics were fixed during fitting.

Differential Scanning Calorimetry (DSC) and Thermogravimetric Analysis (TGA). The differential scanning calorimetric measurements have been carried out on pristine samples in the 175−400 K temperature range at a rate of 10 K min^{-1}. The temperature dependence of the heat flow in the heating and cooling modes for **2**−**22** is shown in SFigure 4 (Supporting Information). The enthalpy associated with the Cr↔S_x transition estimated from the DSC data is reported in STable 1 (Supporting Information). For all compounds, the first heating process reflects structure transformations due to dehydration and concomitant annealing of the samples typical for alkylated compounds. The consequent cooling and the second heating runs give very similar curves, except positions of the peak maxima. In compound **20**, the peak at 270 K might be attributed to pretransition phenomena in the alkyl sublattice, while the peak near 360 K reflects the transition of alkyl chains from an ordered to disordered quasi-liquid state. While in compounds **19** and **21** the melting points are well above 300 K, the Au-containing compound **22** undergoes a high-energetic phase transition at 270 K attributed to an intense peak in the DSC profile and also confirmed by XRPD data (see SFigure 1, Supporting Information). Analogous behavior is also observed for the Ag analogue **17**.

Thermally treated tetracyano Ni, Pd, and Pt derivatives feature broad and poorly defined peaks. We can suggest that the transformation of the ordered alkyl chains with temperature is mechanically hindered due to tethering alkyl chains to a rigid polycyanide framework. Contrary to numerous reported metallomesogens, the melting of **5**, for example, is a process reminiscent of low-energetic

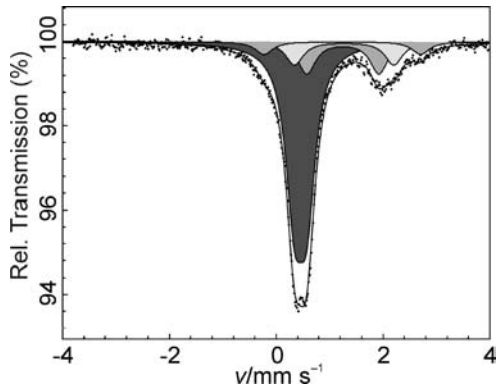

Figure 8. ^{57}Fe Mössbauer spectrum of **3** at 80 K.

second-order phase transitions, as follows also from the gradual change of XRPD profiles with the temperature (SFigure 2, Supporting Information).

Thermogravimetric measurements performed on **1**−**22** show that several samples release water below 400 K, and others only above this temperature, but most of the samples show two-step dehydration processes. There is no clear influence of the content of solvent molecules on the length of alkyl substituents or their number, which points out that water molecules are not involved in donor−acceptor or covalent bonding with any groups of the coordination framework.

Conclusions

We have reported a novel family of 2D Fe(II) metallomesogens exhibiting spin-crossover properties. In contrast with the 2D SCO parent compounds, where the observed spin transitions are of the first order type and accompanied by large hysteresis loops, the metallomesogens present incomplete and continuous spin transition. The apparent loss of cooperativity should be related to the lack of intermolecular contacts between the $[FeM(CN)_4]_\infty$ sheets. In the parent compounds, there are strong $\pi-\pi$ interactions between pyridine and phenyl rings of the ligand molecules of adjacent sheets that lead to strongly cooperative spin transition phenomena.

In the reported metallomesogens, the photo- and thermally induced spin transition and the $Cr\leftrightarrow S_x$ transition take place at different temperature intervals and are consequently classified into type iii. This should not be considered a scientific drawback because it may open new possibilities of research and eventual applications. Investigations of the pressure effect on the spin-crossover properties of an Fe(II) metallomesogen were not yet reported. However, due to the fluid nature of the metallomesogens, one can expect a sensitive response to small pressure changes. Pressure allows tuning of the thermal spin-crossover characteristics in a large range of temperatures.[2b,22] Indeed, application of hydrostatic pressure could place the spin transition in the temperature interval where the $Cr\leftrightarrow S_x$ transition occurs and may lead to interplay/synergy between both phenomena.

Also interesting is the growth/deposition of a single layer of these 2D polymers[23] onto surfaces and the study of their physical and chemical properties. These investigations are prensently going on in our laboratories.

Acknowledgment. We acknowledge the financial help from the Deutsche Forschungsgemeinschaft (Priority Program 1137 "Molecular Magnetism") and the Fonds der Chemischen Industrie. A.B.G. thanks the Spanish MEC for the project CTQ 2007-64727, the FGUVEG (University of Valencia) for a research contract, and the University of Valencia for work-visiting fellowships. We also thank Ms. E. Muth and Ms. P. Räder of the Max-Planck-Institute for Polymer Research, Mainz, for their help in performing TGA and DSC measurements. We are grateful to Dr. R. Dinnebier and Dr. K. Sugimoto, Max-Planck-Institute for Solid State Research, Stuttgart, and Dr. I. Margiolaki for their help in performing high resolution XRPD measurements at the European Synchrotron Radiation Facility (ESRF). We also acknowledge the support of the responsible scientist Dr. E. Welter from HASYLab, Dr. H. Ehrenberg, and Dominic Stürmer from TU Darmstadt during the EXAFS measurements at beamline A1 and A. Michalowicz for providing us with his XAS analysis package.

Supporting Information Available: XRPD patterns of **1**−**22** at different temperatures. ^{57}Fe Mössbauer spectrum of **1**−**13** at 80 K. Differential scanning calorimetry curves for **2**−**17** and **19**−**22**. TGA analysis for **1**−**22**. Enthalpy of the $Cr\leftrightarrow S_x$ transition estimated from the DSC data for **2**−**11**. This material is available free of charge via the Internet at http://pubs.acs.org.

(22) Gütlich, P.; Ksenofontov, V.; Gaspar, A. B. *Coord. Chem. Rev.* **2005**, *249*, 1811.

(23) Sakamoto, J.; van Heijst, J.; Lukin, O.; Schlüter, A. *Angew. Chem., Int. Ed.* **2009**, *48*, 1030.